Immune Response and Pathogen Invasion at the Choroid Plexus in the Onset of Cerebral Toxoplasmosis

Caio Andreeta Figueiredo
OvGU Medizinische Fakultät
JOhannes Steffen
OvGU Medizinische Fakultät
Lorena Morton
OvGU Medizinische Fakultät
Sushmita Arumugam
OvGU Medizinische Fakultät
OLiver Liesenfeld
Charite University Hospital Berlin
Maria A Deli
Hungarian Academy of Science Biological Research Centre
Andrea Kröger
OvGU Medizinische Fakultät
Thomas Schüler
OvGU Medizinische Fakultät
Ildiko Rita Dunay (ildikodunay@gmail.com)
Otto von Guericke Universitat Magdeburg https://orcid.org/0000-0002-9900-8605

Research Article

Keywords: Toxoplasma gondii, neuroinflammation, choroid plexus, blood-CSF barrier, blood-brain barrier, tight junctions, metalloproteinases.

Posted Date: September 27th, 2021

DOI: https://doi.org/10.21203/rs.3.rs-910513/v1

Version of Record: A version of this preprint was published at Journal of Neuroinflammation on January 13th, 2022. See the published version at https://doi.org/10.1186/s12974-021-02370-1.

Immune response and pathogen invasion at the choroid plexus in the onset of cerebral toxoplasmosis

Caio Andreeta Figueiredo[1], Johannes Steffen[1], Lorena Morton[1], Sushmita Arumugam[1], Oliver Liesenfeld[2], Mária A Deli[3], Andrea Kröger[4], Thomas Schüler[5], Ildiko Rita Dunay*[1,6]

[1]Institute of Inflammation and Neurodegeneration, Medical Faculty, Otto-von-Guericke University Magdeburg, Magdeburg, Germany

[2]Institute for Microbiology and Hygiene, Charité Medical School, Berlin, Germany.

[3]Institute of Biophysics, Biological Research Centre, H-6726, Szeged, Hungary;

[4]Institut for Medical Microbiology and Hospital Hygiene, Medical Faculty, Otto-von-Guericke University Magdeburg, Magdeburg, Germany

[5]Institute of Molecular and Clinical Immunology, Medical Faculty, Otto-von-Guericke University Magdeburg, Magdeburg, Germany

[6]Center for Behavioral Brain Sciences – CBBS – Magdeburg, Germany

*** Correspondence:**
Ildiko Rita Dunay
ildikodunay@gmail.com

Abstract

Background: *Toxoplasma gondii* (*T. gondii*) is a highly successful parasite being able to cross all biological barriers of the body, finally reaching the central nervous system (CNS). Previous studies have highlighted the critical involvement of the blood-brain barrier (BBB) during *T. gondii* invasion and development of subsequent neuroinflammation. Still, the potential contribution of the choroid plexus (CP), a main structure forming the blood-cerebrospinal fluid (CSF)-barrier (BCSFB) have not been addressed.

Methods: To investigate *T. gondii* invasion and the onset of neuroinflammation, the CP and brain microvessels (BMV) were isolated and analysed for parasite burden. Additionally, immuno-stained brain sections and three dimensional whole mount preparations were evaluated for parasite localization and morphological alterations. Activation of choroidal and brain endothelial cells were characterized by flow cytometry. To evaluate the impact of early immune

responses on CP and BMV, expression levels of inflammatory mediators, tight junctions (TJ) and matrix metalloproteinases (MMPs) were quantified. Additionally, FITC-dextran was applied to determine infection-related changes in BCSFB permeability. Finally, the response of primary CP epithelial cells to *T. gondii* parasites was tested *in vitro*.

Results: Here we revealed that endothelial cells in the CP are initially infected by *T. gondii,* and become activated prior to BBB endothelial cells indicated by MHCII upregulation. Additionally, CP elicited early local immune response with upregulation of IFN-γ, TNF, IL-6, host-defence factors as well as swift expression of CXCL9 chemokine, when compared to the BMV. Consequently, we uncovered distinct TJ disturbances of claudins, associated with upregulation of MMP-8 and MMP-13 expression in infected CP *in vivo*, which was confirmed by *in vitro* infection of primary CP epithelial cells. Notably, we detected early barrier damage and functional loss by increased BCSFB permeability to FITC-dextran *in vivo*, which was extended over the infection course.

Conclusions: Altogether, our data reveal a close interaction between *T. gondii* infection at the CP and the impairment of the BCSFB function indicating that infection-related neuroinflammation is initiated in the CP.

Keywords: *Toxoplasma gondii*, neuroinflammation, choroid plexus, blood-CSF barrier, blood-brain barrier, tight junctions, metalloproteinases.

1. Background

Toxoplasmosis is a foodborne parasitic disease caused by the obligate intracellular protozoan *Toxoplasma gondii* (*T. gondii*). It is estimated that more than one-third of the world's human population is infected with *T. gondii* and its seroprevalence increases gradually with age (1-3). Following uptake via oral ingestion of contaminated food or water, the parasites proliferate within a variety of nucleated cells, infect circulating leukocytes, successfully cross all the barriers of the body and spread throughout host tissues (4). Despite of the central nervous

system (CNS) being an immune privileged site shielded from peripheral infections and inflammation, *T. gondii* parasites are able to invade the CNS. Previous studies have proposed different mechanisms of parasite invasion, including: (i) active paracellular migration of free parasites, (ii) transmigration of hypermotile infected leukocytes, defined as "Trojan horse" mechanism, and (iii) infection and replication of parasites within brain endothelial cells (5-12). Once parasites cross the brain biological barriers, *e.g.* blood-brain-barrier (BBB), they invade brain-resident cells and persist in cysts lifelong (13-15). The cyst formation within neurons develops a stress-mediated response followed by ongoing basal neuroinflammation, which leads to altered neuronal function, and potentially to behavioral alterations and neuropsychiatric diseases (16-19). In immunodeficient individuals, the infection can lead to disruption of tissue cysts and uncontrolled parasite proliferation, resulting in toxoplasma encephalitis (TE) (2, 20, 21).

Several studies have demonstrated the decisive involvement of the BBB in the invasion of *T. gondii* and the ensuing development of neuroinflammation (reviewed by (22, 23)). In fact, the choroid plexus (CP) is another barrier and potential interface for pathogen invasion into CNS. The CP is the main structure forming the blood-CSF-barrier (BCSFB), and is crucial for CNS homeostasis and cerebrospinal fluid (CSF) secretion. Located within the four brain ventricles, the CP is a villous and selective organ formed by adjacent epithelial cells anchored to a basal lamina and an inner core of resident immune cells surrounding a dense vascular network of fenestrated endothelial cells. Choroidal epithelial cells are tightly interconnected by tight junction proteins (TJ), and control the molecular and cellular composition of the CSF (24, 25). The ability of this unique neuro-immune interface to actively integrate signals between brain and periphery is fundamental to CNS immunity (26), in which CP regulation of immune cell trafficking is considered a central point in the initiation of inflammatory brain responses (27). Alterations or even disruption of the CP epithelium in response to stressful events have detrimental effects on barrier permeability compromising the BCSFB functions (28). Indeed,

BCSFB breakdown has been implicated in neurodegenerative diseases (29-33) and during infection-induced inflammation (31, 34), often indicating the involvement of matrix metalloproteinases (MMPs). Moreover, recent studies have described that the BCSFB serves as a hotspot for direct pathogen infiltration into the CNS (35). However, data concerning the contribution of the CP to *T. gondii* invasion, and subsequent neuroinflammation are controversial and incomplete. For example, the analysis of postmortem samples from immunodeficient patients with cerebral toxoplasmosis identified the CP as a site of infection (36). On the contrary, models of reactivated TE indicate no evidence for the involvement of CP in systemic parasitic dissemination (37, 38).

Here, we demonstrate that, prior to the activation of endothelial cells in the BBB, parasites invading the CNS rapidly seize choroidal endothelial cells. As a result, a prompt immune response is initiated in the CP as shown by the upregulation of cytokines, chemokines, and host-defense-factors, followed by the expression of MMPs, TJ disturbance of CP epithelial cells, and subsequent increased barrier permeability. Together, our results show that the infection takes place in the CP, and indicate sudden functional impairment of the BCSFB upon the onset of the CNS invasion by *T. gondii*.

2. Methods

2.1. Mice and infections *in vivo*

Experiments were conducted with female C57BL/6J mice (8-14 weeks old, purchased from Janvier, Cedex, France). All animals were group-housed in a 12h day/night cycle at 22°C with free access to food and water under specific-pathogen-free conditions and according to institutional guidelines approved by the Animal Studies Committee of Saxony-Anhalt. In order to investigate early *T. gondii* infection, mice were infected by intraperitoneal (*i.p.*) injection of either cysts or tachyzoites. For cyst infection, 2 cysts of the type II ME49 strain harvested from the brains of female NMRI mice infected *i.p.* with *T. gondii* cysts 6-12 months earlier were used

as previously described (39). For tachyzoites infection, type II *T. gondii* reporter parasites of the PTG-GFPS65T strain were grown in monolayers of human foreskin fibroblast (HFF) with DMEM medium (FG0435, Biochrom, Germany), supplemented with 10% fetal bovine serum (FBS) (ThermoFisher, Germany), 1% Penicillin/Streptomycin (Pen/Strep; Sigma, USA) and 1% non-essential amino acids (NEEA) (ThermoFisher, Germany) as previously described (40). Freshly egressed parasites were filtered through a 5 µm Millex-SV syringe filter (Millipore, Germany), and the number of living tachyzoites determined by counting under a light microscope using Trypan Blue 0.4%. Mice were infected *i.p.* with 1 x 10^5 reporter parasites in 200 µl PBS.

2.2. Organ isolation

Mice were deeply anaesthetized by isofluorane inhalation (Baxter), the CSF was collected and thereafter animals were transcardially perfused with 60 ml PBS. For immunofluorescence samples, perfusion was additionally done with 20 ml of 4% paraformaldehyde (PFA) in PBS. Brain, spleen and spinal cord were removed and stored in sterile ice-cold PBS or RNAlater (Sigma) for further processing. Samples stored in RNAlater were kept at 4 °C overnight and afterwards transferred to -80 °C.

2.3. Cerebrospinal fluid collection

CSF was collected by the *cisterna magna* puncture technique as described elsewhere (41). In short, deeply anaesthetized animals were immobilized in a prone position with the head forming a 135° angle with the body, and a sagittal incision of the skin was made inferior to the occiput. Using a stereomicroscope (Stemi 305; ZEISS), the subcutaneous tissue and muscles were dissected, and a glass capillary tube was introduced into the *cisterna magna* through the dura matter, lateral to the arteria *dorsalis spinalis*. An average of 15 µl of CSF per animal were

collected, and kept on ice until further processing. Samples were macroscopically assessed for blood contamination, and discarded when contamination was detected.

2.4. Choroid plexus and brain tissue isolation

Isolated brains were placed under a stereomicroscope in dissection buffer containing HBSS (ROTI®Cell, Roth), and 10 mM HEPES (Gibco, ThermoFisher). CPs were isolated from the lateral, third and fourth brain ventricles, and were either processed for total RNA/DNA isolation, or placed in digestion buffer for further cell isolation. Cerebellum, olfactory bulbs, and adjacent brain meninges were removed and discarded. The remaining brain tissue was used for cell isolation followed by flow cytometric analysis, or further utilized for brain microvessels isolation.

2.5. Brain microvessels isolation

Brain microvessels were isolated as previously described (42) with a few modifications, and used for immunofluorescence, or total RNA/DNA isolation. Briefly, brain hemispheres were minced with a scalpel, and homogenized in digestion buffer (HBSS, with 6.75 g/l glucose, 20 mM HEPES) containing 1 mg/ml DNAse I. After incubation (10 min, 37 °C), homogenate was washed in FACS buffer (PBS w/o Ca/Mg, 2 mM EDTA, 2% v/v FBS, 10 mM HEPES). The resultant pellet was re-suspended and separated by successive centrifugation in 20% (w/v) bovine serum albumin (BSA)-DMEM/F12 solution. To remove remaining myelin debris, the pellet containing microvessels was re-suspended in PBS, fractioned on 22% (v/v) Percoll® (Sigma, #GE17089101) gradient solution and centrifuged for 10 min, 600 g, w/o brake. The microvessels pellet was recovered and extensively washed in PBS/HEPES.

2.6. Cell isolation

Isolated CP and remaining brain tissue were further processed in order to obtain single cell suspensions. CP samples were incubated (20 min, 37 °C) in digestion buffer (PBS w/ Ca/Mg, 2% v/v FBS, 10 mM HEPES) containing 1 mg/ml DNAse I (Sigma, #DN25) and 1 mg/ml Collagenase/Dispase (Sigma, #11097113001). Digested tissues were mechanically dissociated using syringes connected to 22- and 26G needles, then cells were washed with FACS buffer, and used for further analysis. For the isolation of brain cells, hemispheres were minced with a scalpel, and homogenized in digestion buffer (HBSS, with 6.75 g/l glucose, 20 mM HEPES) containing DNAse I and Collagenase/Dispase as previously mentioned. Homogenate was incubated (40 min, 37 °C, 200 rpm), and filtered through a 70 μm cell strainer (Falcon®, #352350). The cell suspension was centrifuged (400 g, 10 min, 4 °C), and the cell pellet separated in a 25-70% discontinuous Percoll® gradient for 20 min without brake. Cells were recovered from the gradient interface, washed with FACS buffer, and used for further analysis.

2.7. Flow-cytometric analysis

Cells were resuspended in FACS buffer, and stained as previously described (39, 40). All antibodies were purchased from BioLegend unless otherwise stated. In short, cells were incubated with an anti-mouse CD16/32 antibody (clone 93, BioLegend, 101302) and stained with fixable viability dye ZombieNIR, for 20 min at 4°C. Subsequently, cells were stained (30 min, 4 °C) using fluorochrome-conjugated antibodies CD11b (PerCP-Cy5.5) eBioscience, CD45 (BV510), MHCII (BV711), and CD31 (APC) BD Biosciences. Cells were washed (400 g, 5 min 4°C) with FACS buffer, fixed in 4% PFA for 15 min at 4 °C and re-suspended in FACS buffer. For CP, cells were additionally permeabilized with eBioscience™ Permeabilization Buffer (Invitrogen), incubated with antibody rabbit-anti-TTR (Abcam) for 40 min, and stained with secondary antibody anti-rabbit AF488 (ThermoFisher). Cells were

acquired using Attune NxT Flow Cytometer (Thermo Fischer). Data was analysed using FlowJo software (version 10.5.3, FlowJo LLC, OR, USA).

2.8. FITC-dextran permeability assay

BCSFB and BBB permeability were measured as previously described (34) with modifications. In short, 4 kDa FITC-dextran (Sigma, #46944) was diluted in PBS, and administered intravenously (*i.v.*) at 75 mg/kg body weight mice, 30 min before CSF and brain collection. CSF was collected through the *cisterna magna* as previously described, diluted 100-fold in PBS, and spun down (1000 g, 5 min). The resulting supernatant were further used for analysis. After perfusion, isolated brains were weighted, minced with a scalpel, homogenized in formamide (Roth) at 0.8 ml per 100 mg tissue, and incubated overnight (37 °C, 200 rpm). Homogenates were spun down (12,000 g, 5 min), and supernatants were collected and diluted 2-fold in PBS. All samples were measured in triplicates at $\lambda_{ex}/\lambda_{em}$ = 485/520 nm using SpectraMaxM5e (Molecular Devices LLC).

2.9. Choroid plexus epithelial cells and *T. gondii in vitro* infection

Primary CP epithelial cell culture was obtained as previously described (43, 44) with modification. Isolated CP from 9 to 14 mice, one week-old, were used in each preparation. Tissues were pooled in digestion buffer (PBS w/ Ca/Mg, 2% v/v FBS, 10 mM HEPES) containing 1 mg/ml DNAse I and 2 mg/ml Collagenase/Dispase, and incubated (20 min, 37 °C). Digested tissues were mechanically dissociated and cells were washed (400 g 5 min) with FACS buffer (PBS w/o Ca/Mg, 2mM EDTA, 2% v/v FBS, 10 mM HEPES). Cell pellet was re-suspended, and cultivated with complete medium (DMEM/F12, supplemented with 10% FBS, 1% Penicillin/Streptomycin, 1% ITS (Insulin-Transferrin-Selenite), 40 mg/ml human-EGF (epidermal growth factor, PeproTech, Germany, #AF-100-15). Cells were grown until confluence, for approximately 7 to 10 days, in 12 well plates previously coated with poly-L-

lysine (PLL), or on top of PLL coated coverslips. Once confluent, cells were infected at multiplicity of infection (MOI) = 5 with type II PTG-GFPS65T tachyzoites, and incubated at 37 °C. After 6 h, culture medium was removed, cells were washed with PBS, and further used for total RNA/DNA isolation, flow cytometric analysis (validation) or immunofluorescence. Naïve controls were treated with pre-warmed fresh medium.

2.10. Immunofluorescence

Immunofluorescence staining was performed for CP whole mount, BMV mount, brain sections and cell culture coverslips. For brain sections, isolated brains were post-fixed (4 h, at 4 °C), soaked in 30% sucrose in PBS (2 days, at 4 °C), and frozen in cryo media (OCT Compound, Tissue Tek). Coronal sections (20 µm) were obtained (Thermo Scientific CryoStar NX50) and only sections containing CP were stained. BMV mount, brain sections and coverslips were stained directly on glass slides. CP whole mount staining were performed utilizing a free-floating approach. All samples from different origins were stained and mounted with the same protocol unless otherwise stated. In short, samples were fixed (4% PFA in PBS, 20 min, 4 °C), washed twice with washing solution (PBS 0.1% (v/v) Triton X-100), and blocked/ permeabilized with PBS 0.3% (v/v) Triton X-100 5% normal-goat-serum (NGS) and unconjugated F(ab´)2-Goat anti-Mouse IgG (H+L) antibody (1:500, Thermo Scientific), for 2 h at 4 °C. Next, samples were incubated with antibody solution (PBS 0.1% (v/v) Triton X-100 2% NGS) containing the primary antibodies of interest: anti-SAG1 (1:50), anti-GFP (1:1000), anti-E-cadherin (1:500), anti-PDGFRβ (1:200), anti-ZO-1(1:50), anti-IBA-1(1:500), anti-CD31 (1:50), and anti-Claudin-2 (1:500). Primary antibodies were incubated overnight at 4 °C, then samples were washed twice, and incubated (30 min, RT) in antibody solution with secondary antibodies (1:1000) tagged with AF488, AF555, AF594 and AF647. Next, samples were washed twice, and mounted with ProLong™ Gold Antifade Mountant with DAPI (ThermoFisher). In some samples, anti-CD45 antibody conjugated with AF647 was used, and

an additional final staining step was added. For brain sections, antigen retrieval (10 mM citrate buffer, pH 6.0, 0.1% Tween-20) was performed at 96 °C for 30 min, before the blocking and permeabilization step. Images were generated using a Leica TCS SP8 microscope, and analysed using the ImageJ software (ImageJ 1.52p).

2.11. DNA and RNA isolation

Total DNA and RNA were isolated from CP, BMV, spleen, spinal cord, brain and CP epithelial cell culture. Samples from CP, BMV and CP epithelial cell culture were isolated with Quick-DNA/RNA Miniprep kit (Zymo Research, Germany) according to the manufacturer's instructions. Brain, spinal cord, and spleen samples were first homogenized with TriFast (Peqlab, 30-2010) using tubes containing Zirconium oxide beads (Precellys, P000926-LYSK0-A) in a BeadBug 6 homogenizer (Biozym). DNA was isolated from the homogenate according to the manufacturer's instructions. RNA was isolated from the homogenate by isopropanol precipitation or using peqGOLD total RNA kit (Peqlab) following the manufacturer's instructions. The concentration and purity of DNA and RNA samples were determined using NanoDrop 2000 spectrophotometer (ThermoFisher; Germany), and samples were stored at -80 °C until further use.

2.12. qPCR

Parasite burden was assessed in triplicates using 40 ng of isolated DNA, FastStart Essential DNA Green Master and LightCycler® 96 System (both Roche, Germany), as previously described (40). Thermal-cycling parameters were set as follows: initial activation (95 °C, 10 min), 55 amplification cycles consisting of denaturation (95 °C, 15 s), annealing (60 °C, 15 s) and elongation (72 °C, 15 s). The DNA target was the published sequence of the highly conserved 35-fold-repetitive B1 gene of *T. gondii* (45, 46). Murine argininosuccinate lyase (*Asl*) was used as reference gene for normalization and relative DNA levels were determined by the

ratio *gene of interest* / *reference gene* and subsequently normalized to mean values of control group (47). Primers were synthetized by Tib MolBiol (Germany) and used at 200 nM final concentration. Primer sequences are described elsewhere [see Additional file 1].

2.13. RT-qPCR

Gene expression levels of cytokines, inflammatory mediators, host-defense factors, tight junctions and MMPs were assessed in triplicates using 20 ng total RNA, TaqMan® RNA-to-C_T™ *1-Step* Kit (Applied Biosystems, Germany) and LightCycler® 96 (Roche, Germany) as previously described (40). Thermal-cycling parameters were set as follows: reverse transcription (48 °C, 30 min), inactivation (95 °C, 10 min) followed by 55 cycles of denaturation (95 °C, 15 s) and annealing/extension (60 °C, 1 min). Utilized TaqMan® Gene Expression Assays (Applied Biosystems, Germany) are listed elsewhere [see Additional file 1]. *Hprt* was chosen as reference gene and relative mRNA levels were determined by the ratio *gene of interest / reference gene* and subsequently normalized to mean values of control group.

For the genes analyzed using SYBR Green technology, Power SYBR® Green RNA-to-CT™ 1-Step Kit (Applied Biosystems, Germany) was used. Samples were analyzed in triplicates (20 ng of isolated mRNA per reaction) using LightCycler® 96 with the following parameters: reverse transcription (48 °C, 30 min), inactivation (95 °C, 10 min) followed by 55 cycles of denaturation (95 °C, 15 s) and annealing/extension (60 °C, 1 min) and melting curve analysis. The primer sequences are listed elsewhere [see Additional file 1] and were synthetized by Tib MolBiol and used at 100 nM final concentration. *Hprt* was chosen as reference gene and relative mRNA levels were determined by the ratio *gene of interest / reference gene* and subsequently normalized to mean values of control group.

2.14. Statistical analysis

Results were statistically analyzed using GraphPad Prism 7 (GraphPad Software Inc., USA), *post-test* corrections were applied according to software recommendations. Statistical significance was set to $p \leq 0.05$. All data are presented as arithmetic mean and standard error of the mean (SEM) and are representative of at least two independent experiments. For parasite burden analysis, normalized data were analyzed by multiple *t*-test, with Holm-Šidák correction for multiple comparisons. For flow cytometric analyses, normalized data were analyzed by one-way ANOVA, with Tukey's correction. For RT-qPCR, data were analyzed by one-way ANOVA followed by Dunnett's correction. BCSFB permeability assay was analyzed by multiple *t*-test to compare between BCSFB and BBB, and one-way ANOVA followed by Dunnett's correction was used to compare differences between day 0 and the time-point analyzed from the same barrier type. RT-qPCR data from primary cell culture was analyzed by student *t*-test.

3. Results

3.1. Choroid plexus is infected by *T. gondii* upon the invasion

BCSFB is a gateway to the CNS for different pathogens as well as immune cells under certain inflammatory conditions (26, 35, 48-50). Assuming that the CP is involved in the parasite entry and early immune response upon the invasion of the brain by *T. gondii*, we investigated the presence of parasites in the CNS through the course of infection. As BBB endothelial cells are cellular targets for *T. gondii* (7), we isolated brain microvessels (BMV) and CP **Fig1A** to assess parasite burden over time by PCR. Our results revealed the early presence of parasites on CP at 3dpi (3 days post-infection), which was increased by day 5 and reduced by day 7 **Fig1B.** In the BMV, the parasite burden only strongly increased by day 7 **Fig1B**. Next, CP and BMV of infected animals were isolated and immuno-stained as a three-dimensional whole mount preparation. Within the CP at 5dpi, we detected parasites ($SAG1^+$) associated to immune cells ($CD45^+$). Extracellular parasites were present in the paracellular and

stromal regions between the CP epithelial cells (E-cadherin^{+}) without co-localization with recruited CD45^{+} cells **Fig1C.** In the BMV, parasites were found to be associated to PDGFRβ^{+} pericytes and ZO-1^{+} endothelial cells **Fig1D**, which constitute the main components of cerebral microvasculature forming the BBB (51). Overall, parasites were found in the CP, and apparently more frequently in initial infection at the BCSFB interface than the BBB. Immuno-staining of isolated BMV confirmed the presence of *T. gondii* tachyzoites in BMV at 7dpi, as detected previously by PCR [see Additional file 2]. Spleens were used as controls to monitor the parasite burden levels in the periphery, indicating the usual spread of the parasites throughout tissues [see Additional file 2]. Parasite burden was just detected starting at 7dpi in both brain parenchyma (after CP removal) and spinal cord, evidencing the early infection through the CP and the microvasculature [see Additional file 2].

3.2. Choroid plexus endothelial and immune cells are targeted by *T. gondii*

Given the early presence of *T. gondii* in the CP, we sought to determine the target cell types in this compartment. Therefore, mice were infected *i.p.* with 10e5 tachyzoites of the *T. gondii* strain expressing the fluorescent protein GFP (PTG-GFPS65T). First, we analyzed coronal brain sections showing CP from lateral ventricles and found parasites within the choroidal endothelial cells at 7dpi **Fig2A** [and see Additional file 3]. Indeed, at 7dpi parasites were additionally found in the cortex and the adjacent brain areas [see Additional file 2], simultaneously to the CP [see Additional file 3]. To identify infected immune cells in the BCSFB, isolated CP whole mounts were co-stained for CD45 and CD31. At 3dpi, we observed *T. gondii* parasites associated to immune cells and endothelial cells in the CP **Fig2B**. Of note, recruited amoeboid-shape CD45^{hi} leukocytes did not appear to be associated to parasites, rather a resident stellate CD45^{int} CP macrophages (referred as CP-BAMs (border-associated-macrophages) or epiplexus cells) were co-localized with parasites at this time point [see Additional file 3]. CP endothelial cells were infected with intracellular parasites at 3 and 5dpi, but at 7dpi infected cells were less abundant. Additionally, parasites were also found in the

inner core of the CP parenchyma, suggesting the infection of mesenchymal derived stromal cells. Altogether, our results demonstrate the dynamic infiltration of parasites into endothelial and immune cells of the CP in the early phase of infection, confirming our initial data on parasite burden.

3.3. Early immune response at the choroid plexus prior to the BBB

Pathogens infecting the CP elicit local immune responses which are associated with the activation of endothelial, epithelial and tissue-resident immune cells (35). To characterize the early immune response to *T. gondii* in the CP in more detail, we first compared the MHCII expression on endothelial cells from CP and remaining brain tissue **Fig3A-H**. In agreement with the spatiotemporal differences in pathogen distribution **Fig1**, MHCII upregulation on endothelial cells was first evidenced in the CP followed by later activation of brain endothelial cells **Fig3A-H**. The kinetics of MHCII expression by microglia was comparable to brain endothelial cells and reached maximum levels at 7dpi [see Additional file 4]. Moreover, MHCII expression was analyzed on CP epithelial cells even though less than 10% of the cells express this marker, a significant increase was observed [see Additional file 4]. Of note, total mRNA expression of MHCII (*H2-Aa*) in the CP was also increased during infection [see Additional file 5]. Taken together, choroidal endothelial cells responded earlier to *T. gondii* than brain endothelial cells and microglia, indicating that the CP is a critical interface for early parasite recognition.

To further compare the local inflammatory response in the BCSFB versus the BBB, we analyzed the mRNA expression of pro-inflammatory cytokines which play a central role in host defense upon *T. gondii* infection. Therefore, CP and the BMV were isolated from infected brains and expression of IFN-γ, TNF, and IL-6 were measured **Fig3I**. Compared to the BMV, CP expression of IFN-γ was higher and earlier elevated. BMV only reached comparable IFN-γ levels at 7dpi. TNF was significantly higher in the CP at both 5 and 7dpi and IL-6 levels peaked at 3dpi and was higher in the CP at 7dpi **Fig3I**. We also evaluated the expression of type I

interferon-β (IFN-β, *Ifnb1*), which were highly expressed in the CP [see Additional file 5]. Furthermore, the cell-autonomous immune response against intracellular *T. gondii* infection is mediated by IFN-γ-inducible GTPases, designated as host-defense-factors (*Irgm1, Igtp, Gbp2b*). Following the elevated IFN-γ levels, we detected higher expression of those genes on the CP compared to the BMV **Fig3J**. Previous studies have shown specific immune cell trafficking molecules to be up-regulated on CP epithelial cells in the presence of IFN-γ and TNF (50). Accordingly, CXCL9 expression was higher in CP throughout the observation period. On the contrary CXCL10 was more pronounced in the BMV, and both chemokines were progressively increased during the infection **Fig3K**. At last, M-CSF (macrophage colony-stimulating factor, *Csf1*) and CX3CL1 (fractalkine), which are chemokines involved in monocyte trafficking across the BCSFB (52) were also found up-regulated in the CP at 7dpi, while no alteration was detected for M-CSF on BMV [see Additional file 5]. Of note, ICAM-1 involved in the general trafficking of immune cells was also up-regulated at the CP [see Additional file 5]. Overall, *T. gondii* elicited an early and local immune response at the BCSFB, with the expression of pro-inflammatory cytokines, IFN-γ-inducible GTPases, and leukocyte trafficking molecules.

3.4. Loss of TJ integrity affects BCSFB function in early infection

TJ molecules constitute the main components of the paracellular barrier established by CP epithelial cells, therefore they assume an essential role determining cellular and molecular compounds delivered from blood into CNS (25). To investigate the outcome of *T. gondii* infection at the BCSFB, we analyzed the expression of TJs in isolated CP tissue over the course of infection. Claudins form the majority group of the integral membrane TJ proteins, which establish complex interactions with intracellular linker proteins like zonula occludens proteins (ZO, *Tjp*) (53). Upon *T. gondii* infection at the CP, we detected lower expression levels of Claudin-2, -3, -5, and -11 compared to naïve group, suggesting a TJ alteration **Fig4A**.

Moreover, the breakdown of epithelial barriers has been associated with increased activity of matrix metalloproteinases (MMPs), which were indicated to be detrimental for BCSFB integrity during neuroinflammation (33). Here, infected CP tissue displayed a robust up-regulation of MMP-8 and MMP-13 **Fig4B**, pointing towards a potential involvement of those endopeptidases in the epithelial barrier perturbation upon parasite invasion of the BCSFB. Taken together, the expression levels of claudins and MMPs in the infected CP suggested a barrier disruption. Indeed, immunostaining for claudin-2 on brain sections showed ruffled-shape irregularities (white arrows) on the contour of CP epithelial cells in infected mice, instead of the smooth and continuous staining pattern depicted in naïve CP **Fig4C**. Finally, we determined whether altered TJ and MMP expression patterns affected CP barrier function. For this purpose, a FITC-dextran permeability assay was performed to assess barrier function *in vivo*. The extravasation of the fluorochrome-conjugated polysaccharide was quantified in the CSF for CP integrity, and in the remaining brain homogenate for BBB integrity **Fig4D**. In contrast to the BBB, BCSFB permeability increased over time. A significant difference between both compartments was first visible at 7dpi and further increased from 10dpi to 23dpi. Thus, our results reveal a continuous increase in BCSFB permeability, suggesting long-standing detrimental effects of *T. gondii* infection on CP barrier integrity. Altogether, *T. gondii* infection results in TJs disturbances in the CP, with possible involvement of MMP-8 and MMP-13, culminating in functional loss and increased permeability of the BCSFB.

3.5. Response of choroid plexus epithelial cells to *T. gondii in vitro*

For a more detailed characterization of *T. gondii* infection effects in the CP epithelium, we developed an *in vitro* culture model for murine primary CP epithelial cells. First, we confirmed the ability of the cultivated cells to establish adhesion junctions and express ZO-1 (honeycomb shape) **Fig5A**. In addition, cell cultures were largely devoid of IBA-1$^+$ myeloid cells and contained mainly CD45$^-$ CD31$^-$ E-cadherin$^+$ epithelial cells **Fig5B**. Subsequently, CP

epithelial cells were cultured in the presence or absence of GFP^+ *T. gondii* and the expression of the TJ proteins ZO-1 and claudin-2 were quantified. ZO-1 **Fig5C** and Claudin-2 **Fig5D** showed a poor and non-continuous distribution, characterized by strand breaks and puncta upon infection, compared to naïve controls. Additionally, the gene expression analysis of the cultivated epithelial cells showed no expression of IFN-γ, but increased expression of IFN-γ-receptor (*Ifngr2*) upon infection. The tissue damage-associated cytokines TNF and IL-6 were also upregulated, and the chemokine CCL2, responsible for myeloid cell recruitment was about 60-fold higher on infected cultures **Fig5E**. We also detected a discrete reduction of ZO-1 (encoded by *Tjp1*) expression upon infection, without change and in the levels of claudin-2 and claudin-11 **Fig5F**. In agreement with **Fig4B**, MMP-8 and -13 showed a robust upregulation upon infection, suggesting that CP epithelial cells are relevant source of MMPs **Fig5G**. Overall, these results demonstrate that epithelial cells from CP directly respond to *T. gondii* infection, and contribute to the local inflammatory response and BCSFB damage.

4. Discussion

The pivotal role of the CP in the orchestration of neuroinflammation became evident in the recent years (49, 54-56), and distinct pathogens have been described exploiting the CP as gateway into CNS (35). These microbes cross CNS barriers via paracellular entry, transcellular penetration, or via infected immune cells (“Trojan horse”) (57). The same mechanisms have been proposed for *T. gondii* invasion of the BBB (23), but only few studies have explored the CP as a gateway for *T. gondii* (36).

Here we demonstrate that *T. gondii* was found in the CP at the onset of infection. In a model of reactivated TE, there was no evidence for the involvement of the CP in *T. gondii* dissemination (37, 38). Whether parasites are able to translocate from blood to the CSF, via CP, and further infect CSF-inundated areas (e.g. brain, spinal cord) is still not fully understood. In fact, we have previously described the extent of spinal cord pathology in a model of

423 experimental chronic toxoplasmosis, suggesting that parasites translocate into CSF while the
424 infection progresses (58). Currently, the lack of tools to specifically block parasite entry into
425 one or another barrier presents a major challenge to unveil their respective contributions to the
426 parasite invasion. Here, we propose that CP infection is the initial step to the development of
427 the neuroinflammation, resulting in the disruption of the BCSFB. Evidences show that the
428 collapse of this barrier and its regulatory mechanisms allow immune cells to enter the CNS and
429 initiate neuroinflammatory diseases (27). As the disease evolves, the parasite spread increases
430 *e.g.* through circulation of infected monocytes which simultaneously can cross the CNS via
431 BBB and CP transposition. It is likely that the higher parasite burden on BMV at 7dpi indicate
432 infected embolized monocytes in small CNS capillaries, as suggested by previous studies (59).
433 Our findings suggest that the activation of the CP vasculature is involved in the
434 orchestration of the anti-parasitic immune responses at early time points of infection. We
435 observed that choroidal endothelial cells upregulated MHCII expression in response to *T. gondii*
436 earlier than brain endothelial cells and microglia. Of note, brain endothelial cells have been
437 described to serve as a replicative niche for *T. gondii* invasion of the CNS (7), but whether
438 activated endothelial cells can control parasite replication *in vivo* is still unknown. Vascular and
439 epithelial alterations at the CP, followed by other alterations like reduced choroidal synthesis,
440 transport capacity, and CSF secretion were shown during aging, and were described to be
441 intensified in Alzheimer's disease (60). Our data confirm the CP as an important interface to
442 early pathogen interaction with endothelial cells, likely promoting damage recognition and
443 antigen-presentation.
444 Infections at the BCSFB has proven to promote CNS inflammation, inducing cytokines
445 and chemokine secretion locally, and in the CSF, mediating immune cell activation and
446 recruitment (61). The CP senses CNS injury and rapidly responds to inflammation, upregulating
447 the expression of adhesion molecules and chemokines receptors essential for leukocyte
448 trafficking (50). Upon the establishment of infection at the CP, we have found that *T. gondii*

449 elicited early and local immune response at the BCSFB, with expression of pro-inflammatory
450 cytokines, IFN-γ-inducible GTPases, and leukocyte trafficking molecules. In face of early
451 detection of $CD45^+$ cells associated to *T. gondii* on the CP, we hypothesize that a transient
452 burden of extracellular parasites in the blood likely reach the CP interface, infecting the
453 choroidal endothelial cells and challenging the resident stromal macrophages and epithelial
454 cells. Additionally, IFN-γ, TNF and IL-6 upregulation in the CP of infected mice might be due
455 to the combined action of immune and epithelial cells, which showed elevated levels of gene
456 expression after *in vitro* culture with *T. gondii*. This suggests a direct anti-parasitic, pro-
457 inflammatory response of the CP epithelial cells. However, IFN-γ gene expression was only
458 detectable in the CP *in vivo* but not in isolated CP epithelial cells co-cultured with *T. gondii*.
459 This indicates that IFN-γ expression is restricted to immune cells. Whether they are CP-resident
460 and/or recruited immune cells from the periphery remains to be clarified. IFN-γ-signaling
461 through CP epithelium have been shown to tightly regulate cell recruitment into CNS (50), and
462 probably will determine the immune cell dynamics through the CP upon *T. gondii* infection.
463 Besides, we detected upregulation of IFN-γ-receptor (*Ifngr2*) on *in vitro* infected CP epithelial
464 cells, likely resulting in the increased expression of leukocyte trafficking genes CSF-1,
465 CX3CL1, ICAM-1, CXCL9 and CXCL10, as previous described (50). Moreover, we found
466 CXCL9 more expressed in CP rather than in BMV through the first week of infection. Indeed,
467 CXCL9 is known to induce T-cell activation and recruitment into the brain during cerebral
468 toxoplasmosis (62). Hereby, CXCL9 could be a differential trafficking molecule expressed by
469 the CP to specific modulated the control of *T. gondii* infection.

470 Dysfunctional BCSFB is part of the pathophysiology leading to increased
471 neuroinflammation (32). At the BCSFB, the permeability is determined by TJ, specifically the
472 claudin-family proteins. Claudin-1, -2, -3 are highly expressed in the CP, and have been shown
473 to be sensitive to inflammation (63-66). In our analysis, claudin-2 was downregulated and
474 overall structurally disorganized within CP epithelial cells, displaying a ruffled shape upon

infection. TJ ruffling frequently correlates with increased paracellular permeability caused by altered anchoring into actin filaments (67-69). This anchoring is dependent on the scaffold protein ZO-1, here, also shown to be changed in the infected CP. Accordingly, alterations of claudins and ZO-1 in the CP have also been described in experimental autoimmune encephalomyelitis (EAE) and LPS- sepsis models (70, 71). Of note, the infection of BCSFB by *Trypanosoma brucei* has indicated direct parasite interactions with claudins of the CP, although the mechanisms of how they induce TJs opening is still not known (72, 73). Still, the disruption of the TJ has been associated to the activity of matrix metalloproteinases (MMP), enzymes implicated on BCSFB breakdown in neurodegenerative diseases and bacterial meningitis (29, 74). We detected increased expression levels of the MMP-8 and MMP-13 on the infected CP, with both MMP upregulated on *in vitro* CP epithelial cultures after *T. gondii* infection. Indeed, previous studies have described MMP-8 contribution to BCSFB leakage, and MMP-13 association with TJ dysregulation (31, 75).

Importantly, here we discovered that the CP damage extended to the chronic phase of experimental murine toxoplasmosis, presented by increased BCSFB permeability, which correlates to our previous findings on neuronal impairment during chronic toxoplasmosis (18, 20, 39, 76). Therefore, we propose that the substantial change on the CP permeability has detrimental implications for CSF composition and impairment of the CNS drainage. Both aspects may contribute to the increased neuroinflammation and subsequent neuronal damage during toxoplasmosis.

5. Conclusion

In summary, we detected that the CP is initially infected early after the onset of *T. gondii* infection, where next to CP endothelial cells also immune cells are targeted, determining a rapid inflammatory response and loss of BCSFB integrity and functionality. These processes are likely driven by TJ disturbance of claudins within CP epithelial cells and by MMP activity.

Thus, dysfunctional BCSFB may early enhance and further contribute to *T. gondii*-induced neuroinflammation, therefore emerging as a crucial target for new therapeutic approaches in cerebral infections.

6. Abbreviations

AF488 – Alexa Fluor 488
AF555 – Alexa Fluor 555
AF594 – Alexa Fluor 594
AF647 – Alexa Fluor 647
ANOVA – analysis of variance
BBB – blood-brain barrier
BCSFB – blood-cerebrospinal fluid barrier
BMV – brain microvessels
CCL2 – chemokine (C-C motif) ligand 2
CD – cluster of differentiation
CNS – central nervous system
CP – choroid plexus
CP-BAMS – choroid plexus border-associated macrophages
CSF – cerebrospinal fluid
CX3CL1 – chemokine (C-X3-C motif) ligand 1
CXCL10 – chemokine (C-X-C motif) ligand 10
CXCL9 – chemokine (C-X-C motif) ligand 9
DAAD - Deutscher Akademischer Austauschdienst
DAPI - 4′,6-diamidino-2-phenylindole
DFG - Deutsche Forschungsgemeinschaft
DMEM – Dulbecco's Modified Eagle Medium
DNA – deoxyribonucleic acid
DNAse I – deoxyribonuclease type I
dpi – days post infection
EDTA – ethylenediamine tetraacetic acid
EGF – epidermal growth factor
FACS – fluorescence-activated cell sorting
FBS – fetal bovine serum
FITC – fluorescein isothiocyanate
Gbp2b – Guanylate binding protein 1
GFP - green fluorescent protein
HBSS - Hank's balanced salt solution
HEPES - 4-(2-hydroxyethyl)-1-piperazineethanesulfonic acid
HFF – human foreskin fibroblasts
IBA-1 – ionized calcium binding adaptor molecule 1
ICAM-1 – Intercellular Adhesion Molecule 1

Ifngr2 - IFN-γ-receptor
IFN-β – type I interferon-beta
IFN-γ – interferon gamma
IgG – immunoglobulin G
Igtp – Interferon gamma-induced GTPase
IL-6 – interleukin 6
Irgm1 – Immunity-related GTPase family M protein 1
ITS – insulin-transferrin-selenite
LPS – Lipopolysaccharides
M-CSF – macrophage colony-stimulating factor
MHCII – major histocompatibility complex type II
MMPs – metalloproteinases
MOI – multiplicity of infection
NEEA – non-essential amino acids
NGS – normal goat serum
OCT - optimal cutting temperature
PBS – phosphate-buffered saline
PCR – polymerase chain reaction
PDGFRβ – platelet derived growth factor receptor β
PFA – paraformaldehyde
PLL – poly-L-lysine
RNA – ribonucleic acid
RT – room temperature
RT-qPCR – Quantitative reverse transcription PCR
SAG1 – surface antigen 1
SEM – standard error of the mean
T.gondii –Toxoplasma gondii
TE – toxoplasma encephalitis
Tjp1 – tight junction protein-1
TJs – tight junctions
TNF – tumor necrosis factor
TTR – transthyretin
ZO-1 – zona occludens-1

7. Declarations

7.1. Ethical approval

All animal experiments were approved by the respective authorities (Landesverwaltungsamt Halle, Sachsen-Anhalt, Germany) in accordance with German and European legislation.

7.2. Consent for publication

Not applicable

7.3. Availability of data and materials

The datasets used and/or analyzed during the current study are available from the corresponding author on reasonable request.

7.4. Competing interests

The authors declare no competing interests.

7.5. Funding

This work was supported by the DFG SFB 854 and SPP 1937 to IRD, by the DAAD research grant for doctoral programmes in Germany (n°57214224) and by the *Promotionsstipendium* of the Medizinischen Fakultät Magdeburg to CF.

7.6. Authors' contributions

CAF and SA performed experiments and analyzed data. JS, LM, AK, OL, MAD, TD critically discussed experimental design, provided material and co-edited the manuscript. CAF and IRD conceived experimental design, and wrote the manuscript.

7.7. Acknowledgments

We thank Petra Grüneberg and Dr. Abidat Schneider for the excellent technical assistance, and all lab colleagues indirectly involved on the execution of this work.

8. References

1. Tenter AM, Heckeroth AR, Weiss LM. Toxoplasma gondii: from animals to humans. Int J Parasitol. 2000;30(12-13):1217-58.

599 2. Montoya JG, Liesenfeld O. Toxoplasmosis. Lancet. 2004;363(9425):1965-76.

600 3. Wilking H, Thamm M, Stark K, Aebischer T, Seeber F. Prevalence, incidence
601 estimations, and risk factors of Toxoplasma gondii infection in Germany: a representative,
602 cross-sectional, serological study. Sci Rep. 2016;6:22551.

603 4. Harker KS, Ueno N, Lodoen MB. Toxoplasma gondii dissemination: a parasite's
604 journey through the infected host. Parasite Immunol. 2015;37(3):141-9.

605 5. Barragan A, Sibley LD. Transepithelial migration of Toxoplasma gondii is linked to
606 parasite motility and virulence. J Exp Med. 2002;195(12):1625-33.

607 6. Courret N, Darche S, Sonigo P, Milon G, Buzoni-Gatel D, Tardieux I. CD11c- and
608 CD11b-expressing mouse leukocytes transport single Toxoplasma gondii tachyzoites to the
609 brain. Blood. 2006;107(1):309-16.

610 7. Konradt C, Ueno N, Christian DA, Delong JH, Pritchard GH, Herz J, et al. Endothelial
611 cells are a replicative niche for entry of Toxoplasma gondii to the central nervous system. Nat
612 Microbiol. 2016;1:16001.

613 8. Lachenmaier SM, Deli MA, Meissner M, Liesenfeld O. Intracellular transport of
614 Toxoplasma gondii through the blood-brain barrier. J Neuroimmunol. 2011;232(1-2):119-30.

615 9. Ueno N, Lodoen MB, Hickey GL, Robey EA, Coombes JL. Toxoplasma gondii-
616 infected natural killer cells display a hypermotility phenotype in vivo. Immunol Cell Biol.
617 2015;93(5):508-13.

618 10. Coombes JL, Charsar BA, Han SJ, Halkias J, Chan SW, Koshy AA, et al. Motile
619 invaded neutrophils in the small intestine of Toxoplasma gondii-infected mice reveal a
620 potential mechanism for parasite spread. Proc Natl Acad Sci U S A. 2013;110(21):E1913-22.

621 11. Bhandage AK, Olivera GC, Kanatani S, Thompson E, Lore K, Varas-Godoy M, et al.
622 A motogenic GABAergic system of mononuclear phagocytes facilitates dissemination of
623 coccidian parasites. Elife. 2020;9.

624 12. Olafsson EB, Barragan A. The unicellular eukaryotic parasite Toxoplasma gondii
625 hijacks the migration machinery of mononuclear phagocytes to promote its dissemination.
626 Biol Cell. 2020.

627 13. Ferguson DJ, Graham DI, Hutchison WM. Pathological changes in the brains of mice
628 infected with Toxoplasma gondii: a histological, immunocytochemical and ultrastructural
629 study. Int J Exp Pathol. 1991;72(4):463-74.

630 14. Dubey JP, Lindsay DS, Speer CA. Structures of Toxoplasma gondii tachyzoites,
631 bradyzoites, and sporozoites and biology and development of tissue cysts. Clin Microbiol
632 Rev. 1998;11(2):267-99.

633 15. Dubey JP. History of the discovery of the life cycle of Toxoplasma gondii. Int J
634 Parasitol. 2009;39(8):877-82.

635 16. Parlog A, Harsan LA, Zagrebelsky M, Weller M, von Elverfeldt D, Mawrin C, et al.
636 Chronic murine toxoplasmosis is defined by subtle changes in neuronal connectivity. Dis
637 Model Mech. 2014;7(4):459-69.

638 17. Blanchard N, Dunay IR, Schluter D. Persistence of Toxoplasma gondii in the central
639 nervous system: a fine-tuned balance between the parasite, the brain and the immune system.
640 Parasite Immunol. 2015;37(3):150-8.

641 18. Lang D, Schott BH, van Ham M, Morton L, Kulikovskaja L, Herrera-Molina R, et al.
642 Chronic Toxoplasma infection is associated with distinct alterations in the synaptic protein
643 composition. J Neuroinflammation. 2018;15(1):216.

644 19. Burgdorf KS, Trabjerg BB, Pedersen MG, Nissen J, Banasik K, Pedersen OB, et al.
645 Large-scale study of Toxoplasma and Cytomegalovirus shows an association between
646 infection and serious psychiatric disorders. Brain Behav Immun. 2019;79:152-8.

647 20. Parlog A, Schluter D, Dunay IR. Toxoplasma gondii-induced neuronal alterations.
648 Parasite Immunol. 2015;37(3):159-70.

649 21. Munoz M, Liesenfeld O, Heimesaat MM. Immunology of Toxoplasma gondii.
650 Immunol Rev. 2011;240(1):269-85.

651 22. Matta SK, Rinkenberger N, Dunay IR, Sibley LD. Toxoplasma gondii infection and its
652 implications within the central nervous system. Nat Rev Microbiol. 2021.

653 23. Mendez OA, Koshy AA. Toxoplasma gondii: Entry, association, and physiological
654 influence on the central nervous system. PLoS Pathog. 2017;13(7):e1006351.

655 24. Ghersi-Egea JF, Strazielle N, Catala M, Silva-Vargas V, Doetsch F, Engelhardt B.
656 Molecular anatomy and functions of the choroidal blood-cerebrospinal fluid barrier in health
657 and disease. Acta Neuropathol. 2018;135(3):337-61.

658 25. Castro Dias M, Mapunda JA, Vladymyrov M, Engelhardt B. Structure and Junctional
659 Complexes of Endothelial, Epithelial and Glial Brain Barriers. Int J Mol Sci. 2019;20(21).

660 26. Baruch K, Schwartz M. CNS-specific T cells shape brain function via the choroid
661 plexus. Brain Behav Immun. 2013;34:11-6.

662 27. Fleischer V, Gonzalez-Escamilla G, Ciolac D, Albrecht P, Kury P, Gruchot J, et al.
663 Translational value of choroid plexus imaging for tracking neuroinflammation in mice and
664 humans. Proc Natl Acad Sci U S A. 2021;118(36).

665 28. Engelhardt B, Sorokin L. The blood-brain and the blood-cerebrospinal fluid barriers:
666 function and dysfunction. Semin Immunopathol. 2009;31(4):497-511.

667 29. Rosenberg GA. Matrix metalloproteinases and their multiple roles in
668 neurodegenerative diseases. Lancet Neurol. 2009;8(2):205-16.

669 30. Vandenbroucke RE. A Hidden Epithelial Barrier in the Brain with a Central Role in
670 Regulating Brain Homeostasis. Implications for Aging. Ann Am Thorac Soc. 2016;13 Suppl
671 5:S407-S10.

672 31. Vandenbroucke RE, Dejonckheere E, Van Lint P, Demeestere D, Van Wonterghem E,
673 Vanlaere I, et al. Matrix metalloprotease 8-dependent extracellular matrix cleavage at the
674 blood-CSF barrier contributes to lethality during systemic inflammatory diseases. J Neurosci.
675 2012;32(29):9805-16.

676 32. Demeestere D, Libert C, Vandenbroucke RE. Therapeutic implications of the choroid
677 plexus-cerebrospinal fluid interface in neuropsychiatric disorders. Brain Behav Immun.
678 2015;50:1-13.

679 33. Brkic M, Balusu S, Van Wonterghem E, Gorle N, Benilova I, Kremer A, et al.
680 Amyloid beta Oligomers Disrupt Blood-CSF Barrier Integrity by Activating Matrix
681 Metalloproteinases. J Neurosci. 2015;35(37):12766-78.

682 34. Gorle N, Blaecher C, Bauwens E, Vandendriessche C, Balusu S, Vandewalle J, et al.
683 The choroid plexus epithelium as a novel player in the stomach-brain axis during
684 Helicobacter infection. Brain Behav Immun. 2018;69:35-47.

685 35. Lauer AN, Tenenbaum T, Schroten H, Schwerk C. The diverse cellular responses of
686 the choroid plexus during infection of the central nervous system. Am J Physiol Cell Physiol.
687 2018;314(2):C152-C65.

688 36. Falangola MF, Petito CK. Choroid plexus infection in cerebral toxoplasmosis in AIDS
689 patients. Neurology. 1993;43(10):2035-40.

690 37. Dellacasa-Lindberg I, Hitziger N, Barragan A. Localized recrudescence of
691 Toxoplasma infections in the central nervous system of immunocompromised mice assessed
692 by in vivo bioluminescence imaging. Microbes Infect. 2007;9(11):1291-8.

693 38. Schluter D, Barragan A. Advances and Challenges in Understanding Cerebral
694 Toxoplasmosis. Front Immunol. 2019;10:242.

695 39. Dusedau HP, Kleveman J, Figueiredo CA, Biswas A, Steffen J, Kliche S, et al.
696 p75(NTR) regulates brain mononuclear cell function and neuronal structure in Toxoplasma
697 infection-induced neuroinflammation. Glia. 2019;67(1):193-211.

698 40. Figueiredo CA, Dusedau HP, Steffen J, Gupta N, Dunay MP, Toth GK, et al.
699 Immunomodulatory Effects of the Neuropeptide Pituitary Adenylate Cyclase-Activating
700 Polypeptide in Acute Toxoplasmosis. Front Cell Infect Microbiol. 2019;9:154.

701 41. Liu L, Duff K. A technique for serial collection of cerebrospinal fluid from the
702 cisterna magna in mouse. J Vis Exp. 2008(21).

703 42. Nakagawa S, Deli MA, Kawaguchi H, Shimizudani T, Shimono T, Kittel A, et al. A
704 new blood-brain barrier model using primary rat brain endothelial cells, pericytes and
705 astrocytes. Neurochem Int. 2009;54(3-4):253-63.

706 43. Menheniott TR, Charalambous M, Ward A. Derivation of primary choroid plexus
707 epithelial cells from the mouse. Methods Mol Biol. 2010;633:207-20.

708 44. Lazarevic I, Engelhardt B. Modeling immune functions of the mouse blood-
709 cerebrospinal fluid barrier in vitro: primary rather than immortalized mouse choroid plexus
710 epithelial cells are suited to study immune cell migration across this brain barrier. Fluids
711 Barriers CNS. 2016;13:2.

712 45. Burg JL, Grover CM, Pouletty P, Boothroyd JC. Direct and sensitive detection of a
713 pathogenic protozoan, Toxoplasma gondii, by polymerase chain reaction. J Clin Microbiol.
714 1989;27(8):1787-92.

715 46. Lin MH, Chen TC, Kuo TT, Tseng CC, Tseng CP. Real-time PCR for quantitative
716 detection of Toxoplasma gondii. J Clin Microbiol. 2000;38(11):4121-5.

717 47. Butcher BA, Fox BA, Rommereim LM, Kim SG, Maurer KJ, Yarovinsky F, et al.
718 Toxoplasma gondii rhoptry kinase ROP16 activates STAT3 and STAT6 resulting in cytokine
719 inhibition and arginase-1-dependent growth control. PLoS Pathog. 2011;7(9):e1002236.

720 48. Baruch K, Deczkowska A, David E, Castellano JM, Miller O, Kertser A, et al. Aging.
721 Aging-induced type I interferon response at the choroid plexus negatively affects brain
722 function. Science. 2014;346(6205):89-93.

723 49. Baruch K, Ron-Harel N, Gal H, Deczkowska A, Shifrut E, Ndifon W, et al. CNS-
724 specific immunity at the choroid plexus shifts toward destructive Th2 inflammation in brain
725 aging. Proc Natl Acad Sci U S A. 2013;110(6):2264-9.

726 50. Kunis G, Baruch K, Rosenzweig N, Kertser A, Miller O, Berkutzki T, et al. IFN-
727 gamma-dependent activation of the brain's choroid plexus for CNS immune surveillance and
728 repair. Brain. 2013;136(Pt 11):3427-40.

729 51. Helms HC, Abbott NJ, Burek M, Cecchelli R, Couraud PO, Deli MA, et al. In vitro
730 models of the blood-brain barrier: An overview of commonly used brain endothelial cell
731 culture models and guidelines for their use. J Cereb Blood Flow Metab. 2016;36(5):862-90.

732 52. Szmydynger-Chodobska J, Strazielle N, Gandy JR, Keefe TH, Zink BJ, Ghersi-Egea
733 JF, et al. Posttraumatic invasion of monocytes across the blood-cerebrospinal fluid barrier. J
734 Cereb Blood Flow Metab. 2012;32(1):93-104.

735 53. Solar P, Zamani A, Kubickova L, Dubovy P, Joukal M. Choroid plexus and the blood-
736 cerebrospinal fluid barrier in disease. Fluids Barriers CNS. 2020;17(1):35.

737 54. Shechter R, Miller O, Yovel G, Rosenzweig N, London A, Ruckh J, et al. Recruitment
738 of beneficial M2 macrophages to injured spinal cord is orchestrated by remote brain choroid
739 plexus. Immunity. 2013;38(3):555-69.

740 55. Schwartz M, Baruch K. The resolution of neuroinflammation in neurodegeneration:
741 leukocyte recruitment via the choroid plexus. EMBO J. 2014;33(1):7-22.

742 56. Kunis G, Baruch K, Miller O, Schwartz M. Immunization with a Myelin-Derived
743 Antigen Activates the Brain's Choroid Plexus for Recruitment of Immunoregulatory Cells to
744 the CNS and Attenuates Disease Progression in a Mouse Model of ALS. J Neurosci.
745 2015;35(16):6381-93.

746 57. Dando SJ, Mackay-Sim A, Norton R, Currie BJ, St John JA, Ekberg JA, et al.
747 Pathogens penetrating the central nervous system: infection pathways and the cellular and
748 molecular mechanisms of invasion. Clin Microbiol Rev. 2014;27(4):691-726.

749 58. Mohle L, Parlog A, Pahnke J, Dunay IR. Spinal cord pathology in chronic
750 experimental Toxoplasma gondii infection. Eur J Microbiol Immunol (Bp). 2014;4(1):65-75.

751 59. Drewry LL, Jones NG, Wang Q, Onken MD, Miller MJ, Sibley LD. The secreted
752 kinase ROP17 promotes Toxoplasma gondii dissemination by hijacking monocyte tissue
753 migration. Nat Microbiol. 2019;4(11):1951-63.

754 60. Serot JM, Zmudka J, Jouanny P. A possible role for CSF turnover and choroid plexus
755 in the pathogenesis of late onset Alzheimer's disease. J Alzheimers Dis. 2012;30(1):17-26.

756 61. Meeker RB, Williams K, Killebrew DA, Hudson LC. Cell trafficking through the
757 choroid plexus. Cell Adh Migr. 2012;6(5):390-6.

758 62. Ochiai E, Sa Q, Brogli M, Kudo T, Wang X, Dubey JP, et al. CXCL9 is important for
759 recruiting immune T cells into the brain and inducing an accumulation of the T cells to the
760 areas of tachyzoite proliferation to prevent reactivation of chronic cerebral infection with
761 Toxoplasma gondii. Am J Pathol. 2015;185(2):314-24.

762 63. Meoli L, Gunzel D. Channel functions of claudins in the organization of biological
763 systems. Biochim Biophys Acta Biomembr. 2020;1862(9):183344.

764 64. Kratzer I, Vasiljevic A, Rey C, Fevre-Montange M, Saunders N, Strazielle N, et al.
765 Complexity and developmental changes in the expression pattern of claudins at the blood-
766 CSF barrier. Histochem Cell Biol. 2012;138(6):861-79.

767 65. Bhat AA, Syed N, Therachiyil L, Nisar S, Hashem S, Macha MA, et al. Claudin-1, A
768 Double-Edged Sword in Cancer. Int J Mol Sci. 2020;21(2).

769 66. Zhou B, Flodby P, Luo J, Castillo DR, Liu Y, Yu FX, et al. Claudin-18-mediated YAP
770 activity regulates lung stem and progenitor cell homeostasis and tumorigenesis. J Clin Invest.
771 2018;128(3):970-84.

772 67. Saeedi BJ, Kao DJ, Kitzenberg DA, Dobrinskikh E, Schwisow KD, Masterson JC, et
773 al. HIF-dependent regulation of claudin-1 is central to intestinal epithelial tight junction
774 integrity. Mol Biol Cell. 2015;26(12):2252-62.

775 68. Kam KR, Walsh LA, Bock SM, Ollerenshaw JD, Ross RF, Desai TA. The effect of
776 nanotopography on modulating protein adsorption and the fibrotic response. Tissue Eng Part
777 A. 2014;20(1-2):130-8.

778 69. Samak G, Gangwar R, Crosby LM, Desai LP, Wilhelm K, Waters CM, et al. Cyclic
779 stretch disrupts apical junctional complexes in Caco-2 cell monolayers by a JNK-2-, c-Src-,
780 and MLCK-dependent mechanism. Am J Physiol Gastrointest Liver Physiol.
781 2014;306(11):G947-58.

782 70. Shrestha B, Paul D, Pachter JS. Alterations in tight junction protein and IgG
783 permeability accompany leukocyte extravasation across the choroid plexus during
784 neuroinflammation. J Neuropathol Exp Neurol. 2014;73(11):1047-61.

785 71. Marques F, Sousa JC, Coppola G, Falcao AM, Rodrigues AJ, Geschwind DH, et al.
786 Kinetic profile of the transcriptome changes induced in the choroid plexus by peripheral
787 inflammation. J Cereb Blood Flow Metab. 2009;29(5):921-32.

788 72. Mogk S, Meiwes A, Bosselmann CM, Wolburg H, Duszenko M. The lane to the brain:
789 how African trypanosomes invade the CNS. Trends Parasitol. 2014;30(10):470-7.

790 73. Mogk S, Meiwes A, Shtopel S, Schraermeyer U, Lazarus M, Kubata B, et al. Cyclical
791 appearance of African trypanosomes in the cerebrospinal fluid: new insights in how
792 trypanosomes enter the CNS. PLoS One. 2014;9(3):e91372.

74. Leppert D, Leib SL, Grygar C, Miller KM, Schaad UB, Hollander GA. Matrix metalloproteinase (MMP)-8 and MMP-9 in cerebrospinal fluid during bacterial meningitis: association with blood-brain barrier damage and neurological sequelae. Clin Infect Dis. 2000;31(1):80-4.

75. Vandenbroucke RE, Dejonckheere E, Van Hauwermeiren F, Lodens S, De Rycke R, Van Wonterghem E, et al. Matrix metalloproteinase 13 modulates intestinal epithelial barrier integrity in inflammatory diseases by activating TNF. EMBO Mol Med. 2013;5(7):1000-16.

76. French T, Dusedau HP, Steffen J, Biswas A, Ahmed N, Hartmann S, et al. Neuronal impairment following chronic Toxoplasma gondii infection is aggravated by intestinal nematode challenge in an IFN-gamma-dependent manner. J Neuroinflammation. 2019;16(1):159.

Figure Legends

Fig1. Detection of *T. gondii* in the CP. Mice were infected *i.p.* with 2 cysts of *T. gondii* type II ME49 and samples were collected at 5dpi. From brains, CPs were isolated under stereomicroscope, and the remaining brain tissue was processed for isolation of BMVs. (**A**) Representative image of freshly isolated CP and a phase-contrast image of isolated BMV. (**B**) Parasite burden *q*PCR analysis of isolated CPs (blue) and BMVs (red) from the correlated animals, which were infected at the same time, and analysed at 3, 5 and 7dpi. The analysis was performed based on the presence of *B1 gene* of *T. gondii* (*TgB1*) normalized to the murine gene *Asl*. Data were normalized to the mean values of 3dpi, and bar charts show individual values of a representative experiment, and mean +SEM. n = 5 per group. Statistical analysis was performed by multiple *t*-test, with Holm-Sidak correction for multiple comparisons. **$p < 0.01$. (**C**) CP whole mount staining to identify immune cells (CD45, blue), *T. gondii* (SAG1, red) and epithelial cells (E-cadherin, green). Scale bars = 50µm (**D**) BMVs immune-staining to identify pericytes (PDGFRβ, blue), *T. gondii* (SAG1, red), and the tight junction ZO-1 (green). Yellow arrows indicate the co-localization of parasites with CD45+ immune cells, and yellow asterisks *T. gondii* signal alone. Scale bars = 50µm.

Fig2. *T. gondii* infection of endothelial and immune cells in the CP. (**A**) Animals were infected *i.p.* with 1x10e5 *T. gondii* type II PTG-GFP tachyzoites. The brains were isolated at

7dpi, and coronal sections were immune-stained with anti-GFP (green), anti-CD31 (magenta) and DAPI (cyan). First row indicate the location of the CP (magenta rectangle) in the lateral ventricle (VL) according to the mouse brain atlas. Second row magnify the CP area above. Yellow arrowheads indicate the detection of parasites co-localized with endothelial cells (CD31). Scale bars = 50µm (**B**) Isolated CPs from animals infected *i.p.* with 1x10e5 PTG-GFP tachyzoites were immune-stained as whole-tissue mount with anti-CD45 (blue), anti-SAG1 (red), and anti-CD31 (green). Animals were infected at the same time, but tissues were analysed at 3, 5 and 7dpi. Yellow arrows indicate CD45/SAG1 co-localization, showing immune cells carrying parasites through the BCSFB. Arrowheads indicate co-localization of CD31/SAG1, and asterisks represent SAG1 signal alone. GFP signal plus SAG1 staining were detected in the same channel and coloured in red for better visualization. Scale bars = 50µm. CTX=cortex; Cc= corpus callosum; CdP= caudoputamen; LS= lateral septal; VL= lateral ventricle.

Fig3. Initial immune response in the CP and BBB upon *T. gondii* infection. Single live cells from (**A-D**) isolated CP and (**E-H**) brain were analysed by flow cytometry, and the expression of MHCII was evaluated on endothelial cells (CD31+CD45-) from both tissues. Dot plots (**A, E**) represent the gating strategy based on FMO controls. Histograms (**B, F**) provide a visual representation of the temporal MHCII expression levels by endothelial cells over *T. gondii* early phase of infection. Bar charts (**C, G**) show the frequency in % of cells derived from parent population (CD31+CD45-). Bar charts (**D, H**) show MFI values of MHCII expression on the endothelial cells. RT-PCR of total RNA isolated from CP and BMV was performed for (**I**) cytokine expression, (**J**) IFN γ-regulated host-defense factors, and (**K**) chemokines. Data from C, D, G, H show individual values and mean ±SEM, n = 5, *$p < 0.05$, **$p < 0.01$, ***$p < 0.001$, ****$p < 0.0001$ (one-way ANOVA, with Tukey's correction). Data from I, J, K was normalized to naïve (day 0) BMV mean, and individual values as mean ±SEM are shown, n = 2-4, #$p < 0.05$, ##$p < 0.01$, ###$p < 0.001$, ####$p < 0.0001$, (one-way ANOVA, with Dunnett's correction). # indicate significant difference between CP and BMV from the same time-point,

and * indicate significant difference between day 0 and the time-point being analysed from the same tissue.

Fig4. Dysregulated tight junctions in the CP affect BCSFB function during early infection. (**A**) Tight junctions and (**B**) MMP-8, and MMP-13 expression analysis (RT-PCR) of total RNA isolated from CP at 3, 5 and 7dpi. Data show individual values and mean ±SEM, n = 2-5, *$p <$ 0.05, **$p < 0.01$, ***$p < 0.001$, ****$p < 0.0001$ (one-way ANOVA, with Dunnett's correction). (**C**) Immunofluorescence of coronal brain sections stained for identification of Claudin-2 (green) and ZO-1 (red) tight junctions from naïve and 7dpi mice. White squares identify the regions of interest shown in higher magnification in the white upper squares. White arrows indicate different areas of Claudin-2 disturbance. Scale bars = 50µm (**D**) Functional FITC-dextran permeability assay comparing the leakage of the BCSFB (blue) versus BBB (red) throughout the course of infection. Data show mean ±SEM (n=5) for each time point analysed. ****$p < 0.0001$, #$p < 0.05$, #### $p < 0.0001$. # indicate significant difference between BCSFB and BBB from the same time-point (multiple t-test), and * indicate significant differences between day 0 and the time-point being analysed from the same barrier type (one-way ANOVA, with Dunnett's correction).

Fig5. Epithelial CP cells response against *T. gondii in vitro.* (**A**) Representative image of cultured choroid plexus epithelial cells stained for the tight junction ZO-1, and myeloid cell marker IBA-1. (**B**) Flow cytometric validation of cultured epithelial cells, identified as E-cadherin^{+}CD45^{-}CD31^{-}. (**C-D**) Primary cultures of CP epithelial cells were infected for 6h with reporter *T. gondii* type II PRU-GFP tachyzoites at MOI=5, and controls remained non-infected. Cultivated cells were immune-stained for detection of (**C**) ZO-1 (red) and (**D**) Claudin-2 (red). DAPI stained the nucleus (blue). GFP-reporter *T. gondii* (green). Scale bars = 50µm. (**E-G**) Naïve and infected cultures were analysed for gene expression of (**E**) cytokines and *Ifngr2*, (**F**) tight junctions, and (**G**) MMPs. Bar charts show individual mean values of triplicates from a

representative experiment, and the mean +SEM (n = 3) for each time point analysed. Data was normalized by naïve means, besides *Mmp13* which was not detectable on naïve samples *$p <$ 0.05 , **$p < 0.01$(student *t*-test).

Additional files

File name	File format	Title of data	Description of data
Additional file 1	.docx	Oligonucleotide primers used for qPCR and RT-qPCR	-
Additional file 2	.tiff	Detection of *T. gondii* on BMV, brain with removed CP and Spinal cord	legend below
Additional file 3	.tiff	Detection of *T. gondii* in the CP and brain	legend below
Additional file 4	.tiff	MHCII expression by microglia cells and CP epithelial cells	legend below
Additional file 5	.tiff	Complementary gene expression analysis of CP and BMVs	legend below

Additional file 2. Detection of *T. gondii* on BMV, brain with removed CP and Spinal cord. Animals were infected *i.p.* with 2 cysts of *T. gondii* type II ME49. CPs were removed and the remaining brain tissue was processed for isolation of BMVs. (**A**) BMVs from 7dpi were stained to identify pericytes (PDGFRβ), *T. gondii* (SAG1), and the tight junction ZO-1. White square area is shown in higher magnification on the right image, and the yellow arrow points to the disseminated signal for *T. gondii*. (**B**) Parasite burden in spleens of infected mice at 3, 5 and 7dpi. The analysis was performed based on the presence of *B1 gene* of *T. gondii* (*TgB1*) normalized to the murine gene *Asl*. Data were normalized to the mean values of 3dpi, and bar charts show individual values of a representative experiment, and mean +SEM, n = 4.*p < 0.05 (multiple *t*-test, with Holm-Sidak correction). (**C**) Brains were isolated, CP removed, and remaining total brain homogenate was processed for parasite detection. (**D**) Spinal cords from

infected mice were also used to quantify parasite burden. The analysis was performed based on expression of *Sag1* gene normalized to *Hprt* expression. Bar charts show individual values of a representative experiment, and mean +SEM, n = 4 (multiple *t*-test, with Holm-Sidak correction).

Additional file 3. Detection of *T. gondii* in the CP and brain. Animals were infected *i.p.* with 2 cysts of *T. gondii* type II ME49. The brains were isolated, and coronal sections or CP whole mount were immune-stained with anti-SAG1 (light blue), anti-CD31 (red), anti-Ecadherin (green) and DAPI (dark blue). (**A**) Confocal image of parasite detection on endothelial cells at 7dpi. (**B**) Magnified region of interested previously identified by white square. (**C**) Parasites identified in the brain cortex, and white square region is magnified in (**D**). (**E**) Parasites on CP and adjacent brain ventricular areas at 7dpi. (**F**) CP whole tissue mount from animals infected *i.p.* with 1x10e5 *T. gondii* type II PRU-tdTomato tachyzoites, showing detection of parasites inside immune and endothelial cells at 3dpi.

Additional file 4. MHCII expression by microglia cells and CP epithelial cells. Single cells suspensions were discriminated based on FSC-SSC parameters, singlets, and viable cells (Zombie NIR negative). (**A**) Brain cells were gated and identified as microglia ($CD11b^{+}CD45^{int}$), CD45+ immune cells, and double negative (DN) cells. (**B**) Choroid plexus cells were first divided in two main populations based on FSC-SSC. Bigger, viable cells were first defined as CD45-CD31- then positive for the CP epithelial cell marker TTR (transthyretin). Smaller, viable cells were gated as $CD45^{+}CD31^{-}$ immune cells, and $CD45^{-}CD31^{+}$ endothelial cells. (**C**) Representative contour plots showing microglia and (**D**) CP epithelial cells MHCII expression at 7dpi. Bar charts represent the frequency in % of cells from parent population, and MFI values of MHCII expression levels. Data represent individual values and mean ±SEM, n=5, $^{**}p < 0.01$, $^{***}p < 0.001$, $^{****}p < 0.0001$ (one-way ANOVA, with Tukey's correction).

914 **Additional file 5. Complementary gene expression analysis of CP and BMVs.** RT-PCR of
915 total RNA from isolated tissue, for (**A**) MHCII expression on CP, (**B, C**) expression of
916 interferon-beta-1 (*Ifnb1*) and macrophage colony-stimulating factor (*Csf1*), respectively, in
917 isolated CP and BMV. (**D, E**) Expression of fractalkine (Cx3cl1) and intercellular-adhesion-
918 molecule-1 (Icam1) on CP. Data show individual values and mean +SEM, n=3-5, *$p < 0.05$,
919 **$p < 0.01$, ***$p < 0.001$, ****$p < 0.0001$ (A, D, E, one-way ANOVA with Tukey's correction;
920 B, C, one-way ANOVA with Dunnett's correction).

Figures

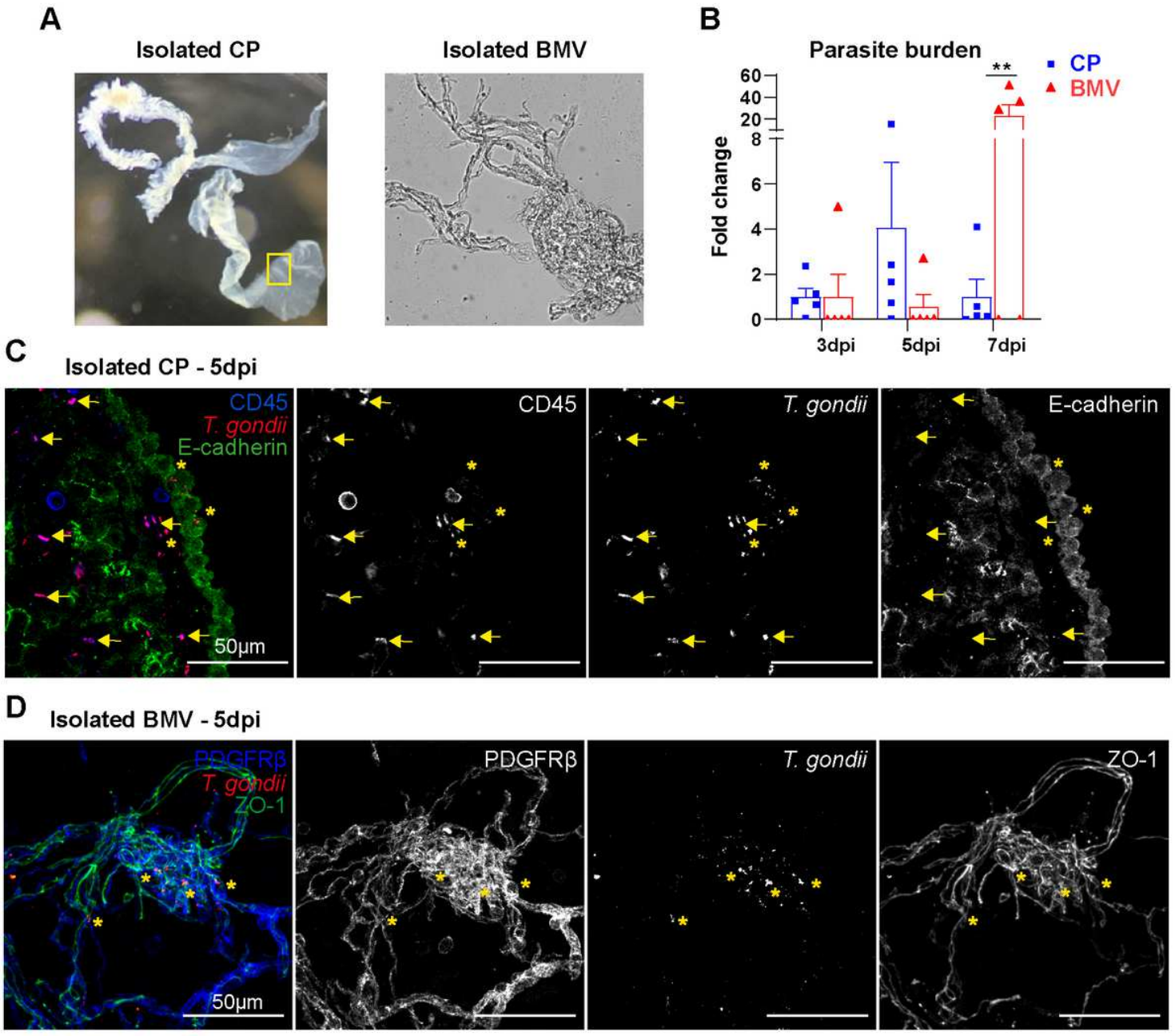

Figure 1

Detection of T. gondii in the CP. Mice were infected i.p. with 2 cysts of T. gondii type II ME49 and samples were collected at 5dpi. From brains, CPs were isolated under stereomicroscope, and the remaining brain tissue was processed for isolation of BMVs. (A) Representative image of freshly isolated CP and a phase-contrast image of isolated BMV. (B) Parasite burden qPCR analysis of isolated CPs (blue) and BMVs (red) from the correlated animals, which were infected at the same time, and analysed at 3, 5 and 7dpi. The analysis was performed based on the presence of B1 gene of T. gondii (TgB1) normalized to the murine gene Asl. Data were normalized to the mean values of 3dpi, and bar charts show individual values of a representative experiment, and mean +SEM. n = 5 per group. Statistical analysis was performed by

multiple t-test, with Holm-Sidak correction for multiple comparisons. **p < 0.01. (C) CP whole mount staining to identify immune cells (CD45, blue), T. gondii (SAG1, red) and epithelial cells (E-cadherin, green). Scale bars = 50µm (D) BMVs immune-staining to identify pericytes (PDGFRβ, blue), T. gondii (SAG1, red), and the tight junction ZO-1 (green). Yellow arrows indicate the co-localization of parasites with CD45+ immune cells, and yellow asterisks T. gondii signal alone. Scale bars = 50µm.

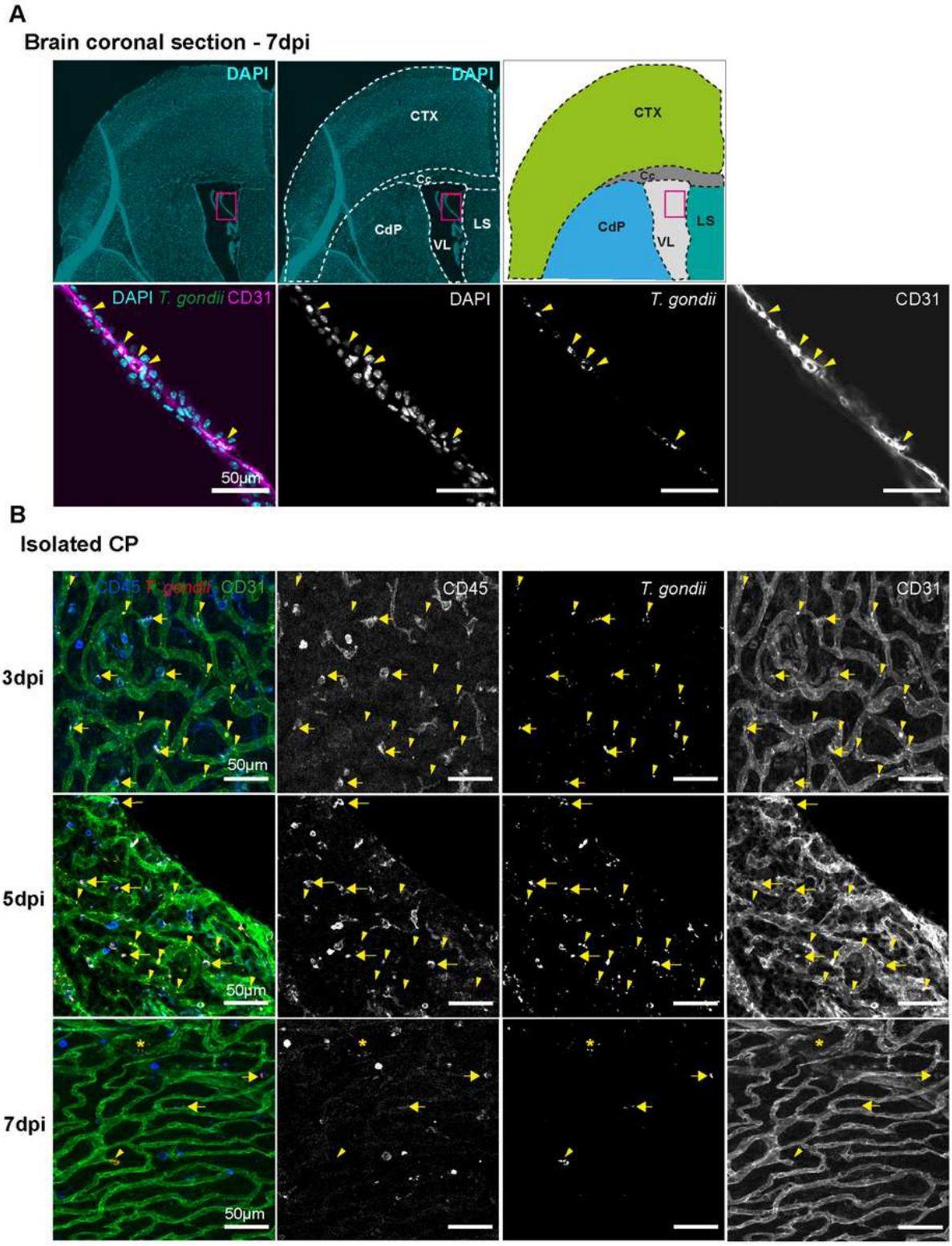

Figure 2

T. gondii infection of endothelial and immune cells in the CP. (A) Animals were infected i.p. with 1x10e5 T. gondii type II PTG-GFP tachyzoites. The brains were isolated at 7dpi, and coronal sections were immune-stained with anti-GFP (green), anti-CD31 (magenta) and DAPI (cyan). First row indicate the location of the CP (magenta rectangle) in the lateral ventricle (VL) according to the mouse brain atlas. Second row magnify the CP area above. Yellow arrowheads indicate the detection of parasites co-localized with endothelial cells (CD31). Scale bars = 50µm (B) Isolated CPs from animals infected i.p. with 1x10e5 PTG-GFP tachyzoites were immune-stained as whole-tissue mount with anti-CD45 (blue), anti-SAG1 (red), and anti-CD31 (green). Animals were infected at the same time, but tissues were analysed at 3, 5 and 7dpi. Yellow arrows indicate CD45/SAG1 co-localization, showing immune cells carrying parasites through the BCSFB. Arrowheads indicate co-localization of CD31/SAG1, and asterisks represent SAG1 signal alone. GFP signal plus SAG1 staining were detected in the same channel and coloured in red for better visualization. Scale bars = 50µm. CTX=cortex; Cc= corpus callosum; CdP= caudoputamen; LS= lateral septal; VL= lateral ventricle.

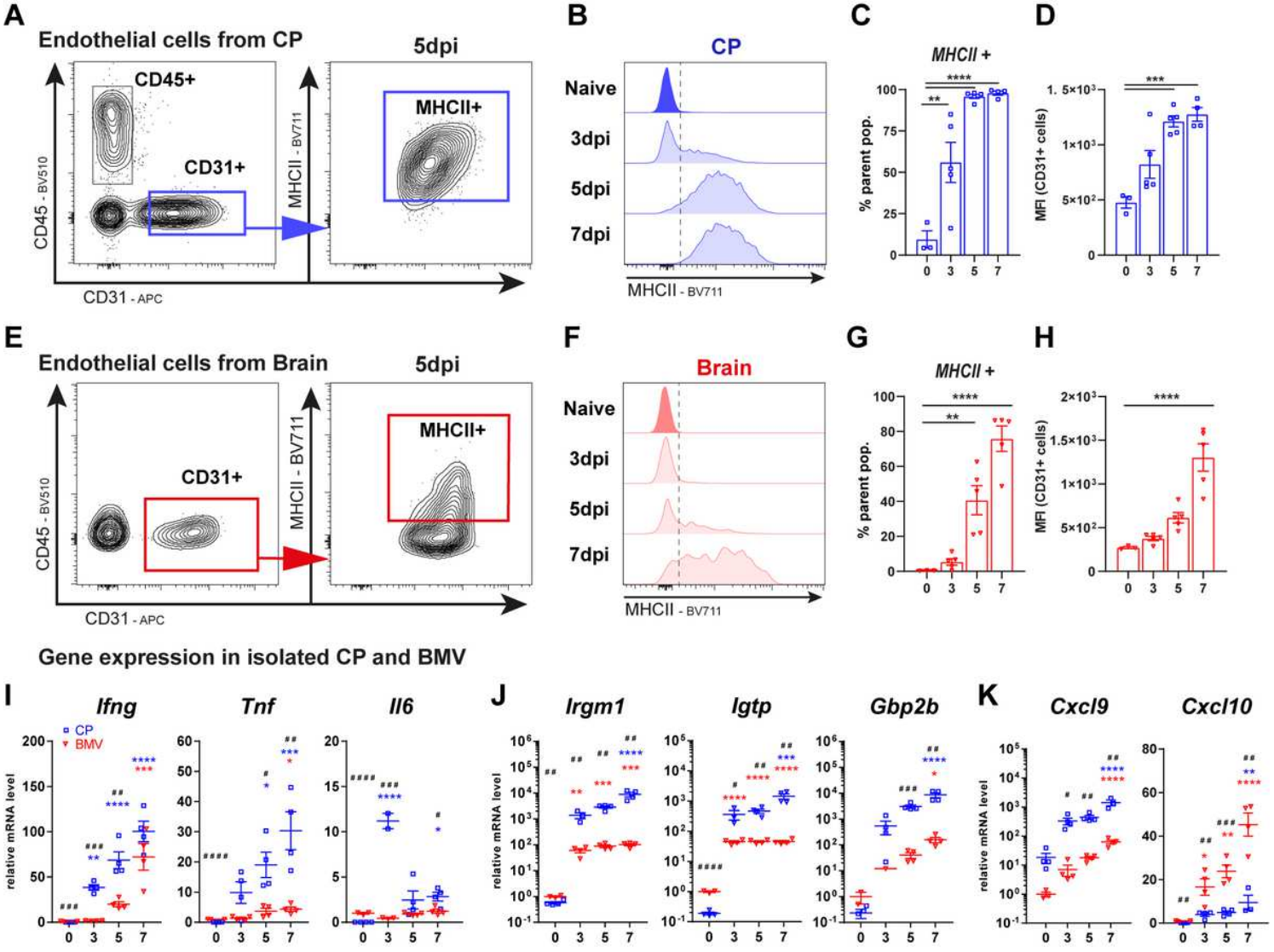

Figure 3

Initial immune response in the CP and BBB upon T. gondii infection. Single live cells from (A-D) isolated CP and (E-H) brain were analysed by flow cytometry, and the expression of MHCII was evaluated on endothelial cells (CD31+CD45-) from both tissues. Dot plots (A, E) represent the gating strategy based on FMO controls. Histograms (B, F) provide a visual representation of the temporal MHCII expression levels by endothelial cells over T. gondii early phase of infection. Bar charts (C, G) show the frequency in % of cells derived from parent population (CD31+CD45-). Bar charts (D, H) show MFI values of MHCII expression on the endothelial cells. RT-PCR of total RNA isolated from CP and BMV was performed for (I) cytokine expression, (J) IFN γ-regulated host-defense factors, and (K) chemokines. Data from C, D, G, H show individual values and mean ±SEM, n = 5, *p < 0.05 , **p < 0.01, ***p < 0.001, ****p < 0.0001 (one-way ANOVA, with Tukey's correction). Data from I, J, K was normalized to naïve (day 0) BMV mean, and individual values as mean ±SEM are shown, n =2-4, # p < 0.05, ## p < 0.01, ### p < 0.001, #### p < 0.0001, (one-way ANOVA, with Dunnett's correction). # indicate significant difference between CP and BMV from the same time-point, and * indicate significant difference between day 0 and the time-point being analysed from the same tissue.

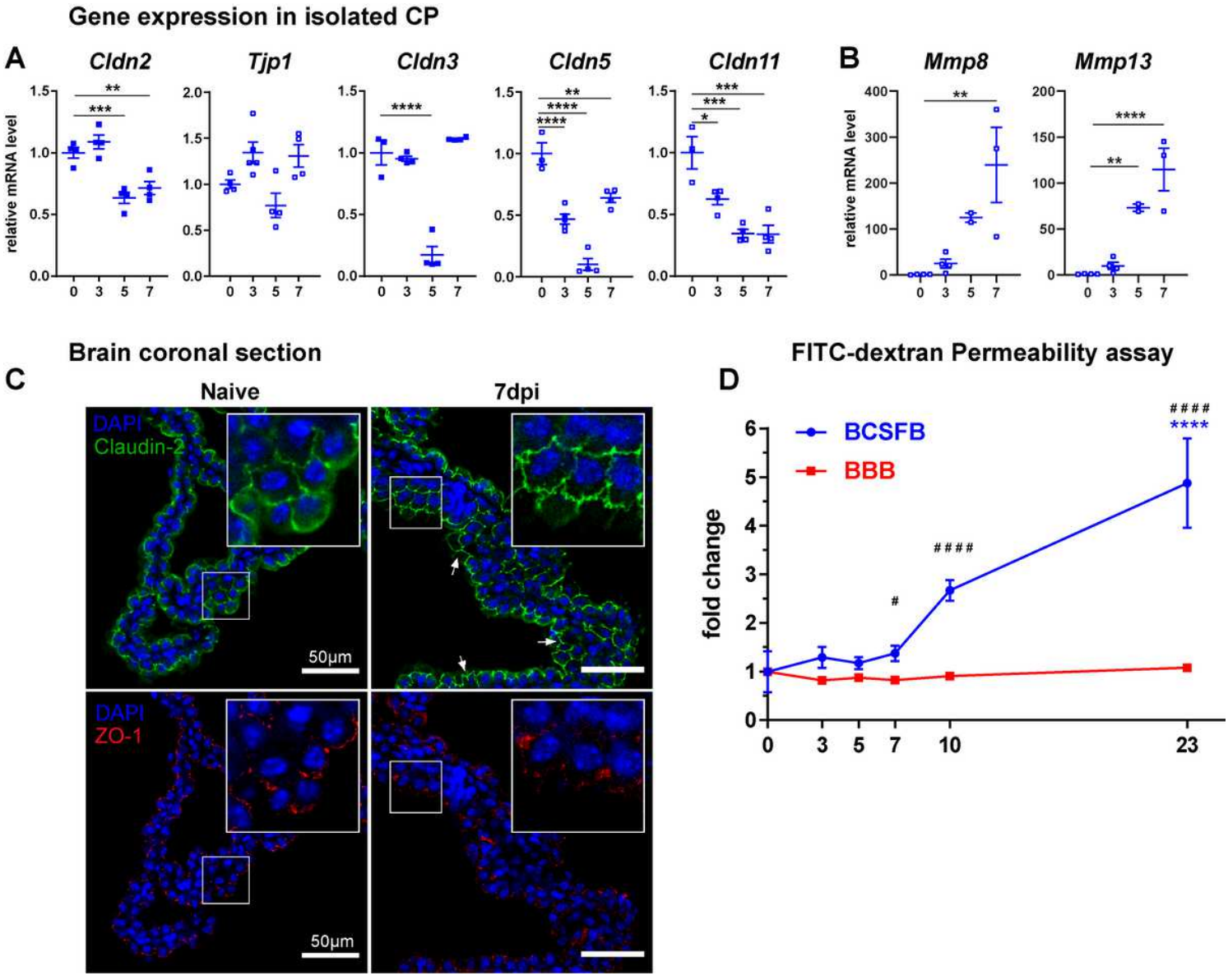

Figure 4

Dysregulated tight junctions in the CP affect BCSFB function during early infection. (A) Tight junctions and (B) MMP-8, and MMP-13 expression analysis (RT-PCR) of total RNA isolated from CP at 3, 5 and 7dpi. Data show individual values and mean ±SEM, n = 2-5, *p < 0.05, **p < 0.01, ***p < 0.001, ****p < 0.0001 (one-way ANOVA, with Dunnett's correction). (C) Immunofluorescence of coronal brain sections stained for identification of Claudin-2 (green) and ZO-1 (red) tight junctions from naïve and 7dpi mice. White squares identify the regions of interest shown in higher magnification in the white upper squares. White arrows indicate different areas of Claudin-2 disturbance. Scale bars = 50μm (D) Functional FITC-dextran permeability assay comparing the leakage of the BCSFB (blue) versus BBB (red) throughout the course of infection. Data show mean ±SEM (n=5) for each time point analysed. ****p < 0.0001, # p < 0.05, #### p < 0.0001. # indicate significant difference between BCSFB and BBB from the same time-point (multiple t-test), and * indicate significant differences between day 0 and the time-point being analysed from the same barrier type (one-way ANOVA, with Dunnett's correction).

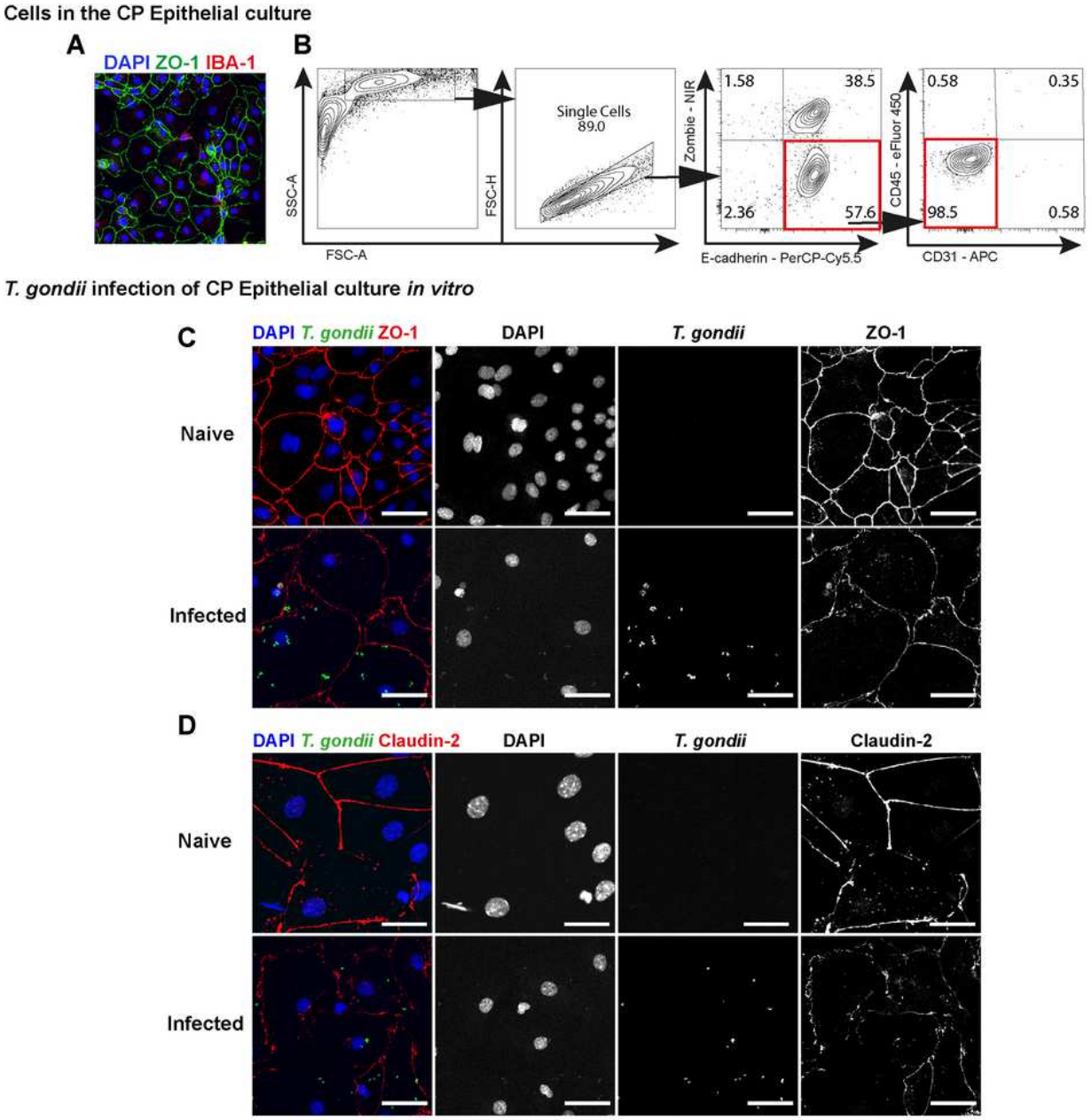

Figure 5

Epithelial CP cells response against T. gondii in vitro. (A) Representative image of cultured choroid plexus epithelial cells stained for the tight junction ZO-1, and myeloid cell marker IBA-1. (B) Flow cytometric validation of cultured epithelial cells, identified as E-cadherin+CD45-CD31-. (C-D) Primary cultures of CP epithelial cells were infected for 6h with reporter T. gondii type II PRU-GFP tachyzoites at MOI=5, and controls remained non-infected. Cultivated cells were immune-stained for detection of (C) ZO-1 (red) and

(D) Claudin-2 (red). DAPI stained the nucleus (blue). GFP-reporter T. gondii (green). Scale bars = 50μm. (E-G) Naïve and infected cultures were analysed for gene expression of (E) cytokines and Ifngr2, (F) tight junctions, and (G) MMPs. Bar charts show individual mean values of triplicates from a representative experiment, and the mean +SEM (n = 3) for each time point analysed. Data was normalized by naïve means, besides Mmp13 which was not detectable on naïve samples *p < 0.05 , **p < 0.01(student t-test).

Supplementary Files

This is a list of supplementary files associated with this preprint. Click to download.

- Additionalfile01tableofoligonucleotides.docx
- Additionalfile02.tif
- Additionalfile03.tif
- Additionalfile04.tif
- Additionalfile05.tif